and were designated MN5-10S, MN5-14S, and MN5Rh-3, respectively. For single-cycle infectivity assays to monitor viral susceptibility to TRIM5 proteins and to determine infectivity for CyM cells, *env*-deficient HIV-1mt variants encoding luciferase gene were constructed. NL-DT5R was cleaved with *Nde*I and *Nhe*I (both sites in *env* gene), blunt ended by T4 DNA polymerase, and resealed by T4 DNA ligase. The resultant clone was designated 5RΔEnv. Luciferase gene was then introduced into *nef* gene of 5RΔEnv as described previously [22], and the resultant clone was designated 5RΔEnv + Luc. A fragment containing the 3′ half genome was cut out from the 5RΔEnv + Luc, and introduced into the corresponding region in HIV-1mt variants (DT5R/4-3, NL-DT5RS, MN4-8, MN4-8S, and MN4Rh-3) to generate 5R/4-3ΔEnv + Luc, 5RSΔEnv + Luc, 4-8ΔEnv + Luc, 4-8SΔEnv + Luc, and 4Rh-3ΔEnv + Luc, respectively.

2.2. Cell culture

A human monolayer cell line 293T [23], a feline kidney cell line CRFK (ATCC CCL-94), and a CyM kidney cell line MK.P3(F) (JCRB 0607) were maintained in Eagles's minimal essential medium (MEM) containing 10% heat-inactivated fetal bovine serum (hiFBS). CRFK cells expressing TRIM5α/TRIMCyp were maintained in MEM containing 10% hiFBS and 400 μg/mL G418 (SIGMA). Macaque lymphocyte cell lines, HSC-F [24] and HSR5.4 [25], were maintained in RPMI-1640 medium containing 10% hiFBS. Recombinant human IL-2 (AbD Serotec) was added to the medium (50 units/mL) for maintenance of HSR5.4 cells. A human lymphocyte cell line MT4/CCR5 (MT4 cells stably expressing CCR5) was maintained in RPMI-1640 medium containing 10% hiFBS and 200 μg/mL hyglomycine (SIGMA).

2.3. Virus replication assays

Virus stocks for infection were prepared from 293T cells transfected with proviral clones as described previously [16,19,26]. Virion-associated reverse transcriptase (RT) activity was measured as described previously [16]. HSC-F cells (10^6) were infected with equal RT units of viruses in the presence of IL-2. For infection of MT4/CCR5 cells (10^6), the spinoculation method [27] was used. Viral growth was monitored by RT activity released into the culture supernatants. We assessed the viral growth potential by the peak day of virus production, and if the viral growth kinetics are similar, by the production level on the peak day.

2.4. Generation and characterization of adapted viral clones

MN4-5S and MN5-10S viruses (Fig. 1) prepared from transfected 293T cells were inoculated into HSR5.4 cells (3×10^6) with an equal amount of viruses (5×10^7 RT units). The cultures were maintained in the presence of IL-2, and HSC-F cells were added on day 34 post-infection. The culture supernatants (collected on day 18 post-cocultivation, the peak day of virus production) were inoculated into fresh HSR5.4 cells, and total DNA was extracted from the cells on day 15 post-infection. Integrated proviruses were amplified from total DNA as two overlapping fragments by the polymerase chain reaction (PCR), and amplified products were cloned into MN5-10S as described previously [16]. Viruses were prepared from 293T cells transfected with the resultant clones, and inoculated into HSR5.4 cells. Only one clone exhibited a rapid growth kinetics compared to MN5-10S, and was designated Ad clone-25. To identify an adaptive mutation that enhances growth potential, each mutation found in the genome of Ad clone-25 was introduced into MN5-14S by site-directed mutagenesis (STRATAGENE). For screening, viruses prepared from transfected 293T cells were inoculated into HSC-F cells, and virus replication was monitored by RT activity released into the culture supernatants.

2.5. Molecular modeling of HIV CA N-terminal domain (NTD)

The crystal structure of HIV-1 CA NTD at a resolution of 2.00 Å (PDB code: 1M9C [28]) was taken from the RCSB Protein Data Bank [29]. The three-dimensional (3-D) models of HIV-1 CA NTD were constructed by the homology modeling technique using 'MOE-Align' and 'MOE-Homology' in the Molecular Operating Environment (MOE) (Chemical Computing Group Inc., Quebec, Canada) as described [30–32]. We obtained 25 intermediate models per one homology modeling in MOE, and selected the 3-D models which were the intermediate models with best scores according to the generalized Born/volume integral methodology [33]. The final 3-D models were thermodynamically optimized by energy minimization using an AMBER99 force field [34] combined with the generalized Born model of aqueous solvation implemented in MOE [35]. Physically unacceptable local structures of the optimized 3-D models were further refined on the basis of evaluation by the Ramachandran plot using MOE.

2.6. Single-cycle infectivity assays

To generate CRFK cells expressing CyM TRIMCyp, the cDNA was isolated from HSC-F cells, and expression vector of FLAG-tagged CyM TRIMCyp was constructed as described previously [18]. The sequence of TRIMCyp from HSC-F cells was identical with Mafa TRIMCyp2 (GenBank: FJ609415). CRFK cell lines expressing CyM TRIMCyp were selected by G418 as described previously [18]. Expression and inhibitory effect of the selected cell clones were verified by Western blotting with anti-FLAG antibody (SIGMA) and by infection with vesicular stomatitis virus G protein (VSV-G) pseudotyped 5R/4-3ΔEnv + Luc, respectively. Assays using naïve CRFK, CRFK expressing CyM TRIM5α [18] or CyM TRIMCyp, and MK.P3(F) cells were similarly performed as described previously [36]. VSV-G pseudotyped virus stocks were prepared from 293T cells transfected with individual HIV-1mtΔEnv + Luc clones and pCMV-G (GenBank: AJ318514)

at a molar ratio of 1:1. Naïve CRFK, CRFK expressing TRIM5α/TRIMCyp and MK.P3(F) cells were infected with an equal titer of viruses (to generate approximately 10^7 relative luminescence (RLU) for naïve CRFK cells), and on day 2 post-infection, cells were analyzed for luciferase activity. Assays using recombinant Sendai virus (SeV)-CyM TRIM5α/TRIMCyp expression system were performed as described previously [31].

3. Results

3.1. An adaptive mutation G114E on helix 6 in CA (CA-G114E) enhances viral growth potential in macaque cells

An HIV-1mt variant MN4-5S replicated more slowly than SIVmac239 in macaque cells. In order to improve its growth potential, we carried out virus adaptation in a macaque lymphocyte cell line HSR5.4. Virus adaptation was performed by long-term culture of HSR5.4 cells infected with MN4-5S (X4-tropic) or its R5-tropic version MN5-10S (Fig. 1). Construction of proviral clones from adapted viruses was described in Materials and methods. We obtained only one clone (Ad clone-25) with enhanced growth potential from 100 proviral clones constructed and tested. We sequenced the entire genome of Ad clone-25, and found three non-synonymous mutations in CA (S33N, G114E, and T147A in Fig. 2A) and one synonymous mutation in integrase (IN)(a4943c in Fig. 2A). To identify an adaptive mutation that enhances growth potential, each mutation found in Ad clone-25 was introduced into a parental clone MN5-14S (Fig. 1). MN5-14S carries only growth-promoting mutations in MN5-10S, and the two clones exhibit similar growth potential in macaque cells. Viruses were prepared from 293T cells transfected with MN5-14S, Ad clone-25, or clones carrying individual mutations, and inoculated into HSC-F cells (Fig. 2A). Only one clone carrying CA-G114E exhibited similar growth kinetics to that of Ad clone-25 but not the others. This result indicates that CA-G114E is an adaptive mutation enhancing growth potential of HIV-1mt in macaque cells. This mutation is exactly the same as the previously found adaptive mutation, which enhanced growth of NL-4/5S6/7SvifS virus in human CEM-SS cells [37]. NL-4/5S6/7SvifS virus is a prototype HIV-1mt bearing the same CA with that of MN4-5S.

3.2. Molecular modeling of the CA NTD of HIV-1mt variants suggests that CA-G114E and CA-Q110D mutations have a similar positive effect on viral replication

The amino acid at position 114 is located in CA NTD. To obtain structural insights into impacts of the G114E substitution in order to improve growth capability of HIV-1mt variants in macaque cells, we conducted computer-assisted structural study: we constructed 3-D models of CA NTD of three HIV-1mt variants, CA-G114E, CA-G114Q, and MN4-5S, using homology-modeling technique (see Materials and methods). Main chain folds of the three models were indistinguishable, suggesting that 3-D position and type of side chain are critical

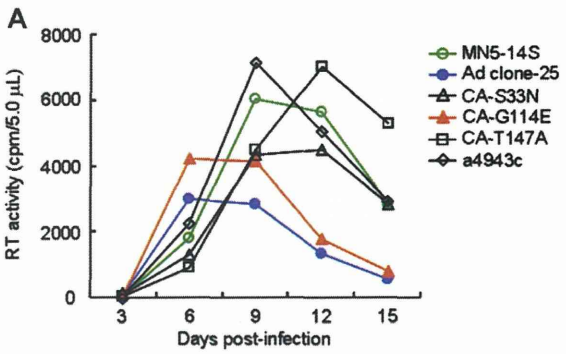

Nucleotide change	Region	Amino acid change in the region
g1283a	CA	S33N
g1526a	CA	G114E
a1624g	CA	T147A
a4943c	IN	None

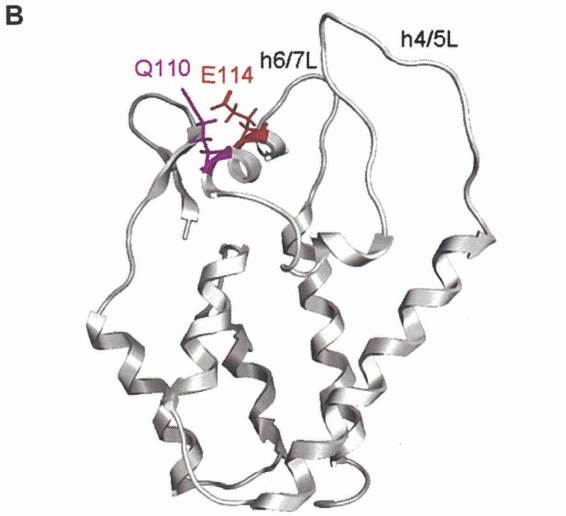

Fig. 2. Mutations in Gag-CA. (A) Identification of an adaptive mutation that enhances viral growth. Nucleotide substitutions found in the genome of Ad clone-25 are indicated at the bottom. Virus samples were prepared from 293T cells transfected with the indicated proviral clones, and equal RT units were inoculated into HSC-F cells. MN5-14S and Ad clone-25 served as controls. Virus replication was monitored by RT activity released into the culture supernatants. (B) 3-D structural models for CA NTD of HIV-1mt variants. Structural models of CA NTD of HIV-1mt variants were constructed by homology-modeling using "MOE-Align" and "MOE-Homology" in MOE as described previously [30–32]. Crystal structure of HIV-1 CA NTD at a resolution of 2.00 Å (PDB code: 1M9C [28]) was used as template for homology modeling. Main chain folds were indistinguishable among the models, and only the model of G114E CA is shown as a representative. Magenta and red sticks: side chains of 110th and 114th amino acid residues, respectively, of the G114E CA NTD.

for the phenotypic change. The modeling study revealed that 114th residue of G114E CA NTD is located on helix 6 in CA NTD such that its side chain protrudes into the exposed surface of CA (Fig. 2B). A charged amino acid residue on a protein surface participates in determining physicochemical properties of interaction surface of the protein and thus influences its structural and functional properties. Therefore, we assumed that the protrusion of a negatively charged side chain from helix 6 into exposed surface could have somehow a positive effect on growth capability of the HIV-1mt variants in macaque cells. In this regard, especially worth noting is that 110th amino acid residue on helix 6 of the HIV-1mt variant CAs was positioned on the same helical face with 114th amino acid residue (Fig. 2B). Therefore, we predicted that substitution of glutamine (Q) at position 110 by acidic amino acid such as aspartic acid (D) and glutamic acid (E) may also have a positive effect on growth capability of the HIV-1mt variants in macaque cells as G114E does. SIVmac239 has aspartic acid and glutamine at the positions 110 and 114, respectively.

3.3. CA-Q110D promotes viral growth more efficiently in macaque cells than CA-G114E mutation but its enhancing effect is species-specific

To confirm our prediction described above, CA-Q110D mutation was introduced into MN5-14S (designated MN5Rh-3), and the growth property in HSC-F cells of MN5Rh-3 and a viral clone carrying G114E (CA-G114E in Fig. 2A) was compared. As shown in Fig. 3A, MN5Rh-3 grew better than CA-G114E, indicating that CA-Q110D further accelerates HIV-1mt replication in macaque cells compared with an adaptive CA-G114E mutation. We next constructed an X4-tropic proviral clone carrying the CA-Q110D (designated MN4Rh-3) (Fig. 1), and compared its growth property with MN5Rh-3 in HSC-F cells (Fig. 3B). MN4Rh-3 was found to exhibit higher growth ability than MN5Rh-3, and was therefore used for infection experiments hereafter.

While CypA and TRIM5α have inhibitory effect on HIV-1 replication in macaque cells, CypA promotes HIV-1 infection in human cells and human TRIM5α only weakly inhibits HIV-1 replication [38–40]. Since the CA-Q110D mutation (acquisition of negatively charged side chain), as predicted by structural modeling, could impact on the interaction of HIV-1 CA and its binding factor(s) by altering physicochemical properties of CA binding surface, it can be speculated that CA-Q110D may promote viral replication specifically in macaque cells. Thus, we analyzed the effect of CA-Q110D on viral growth in macaque and human cells. In this experiment, we used HIV-1mt variants (MN4-8, MN4-8S, and MN4Rh-3) that have distinct CA structures (Fig. 1). Viruses prepared from transfected 293T cells were inoculated into macaque HSC-F and human MT4/CCR5 cells, and examined for growth property (Fig. 3C). The introduction of SIVmac239 CA h6/7L (MN4-8S) resulted in enhanced and reduced viral growth in macaque and human cells, respectively, relative to MN4-8. MN4Rh-3 grew clearly better in macaque cells relative to MN4-8 and MN4-8S, but more poorly in human cells than the other twos. These results demonstrate that the CA-Q110D mutation enhances viral replication in a host cell species-specific manner.

3.4. CA-Q110D does not contribute to evasion from CyM TRIM5 proteins restriction

We predicted that the growth enhancement by CA-Q110D may come from the increased resistance to CyM TRIM5 proteins, and therefore examined the susceptibility of HIV-1mt variants to them by two independent assays.

First, assays were performed in feline kidney CRFK cells expressing TRIM5α or TRIMCyp by using VSV-G pseudotyped viruses encoding the luciferase gene (Fig. 4A–C). The sequence differences between HIV-1mt variants reside only in CA and IN (Figs. 1 and 4). Since adaptive mutations in IN contribute to enhancement of virion production but not early replication phase (manuscript in preparation), only the difference in CA affects the relative single cycle infectivity in this assay. A pseudotyped virus 5R/4-3 carries HIV-1 (NL4-3) CA without any modifications and served as negative control. While 5R and 4-8 have an identical CA structure carrying h4/5L from SIVmac239, 5RS and 4-8S have both h4/5L and h6/7L from SIVmac239 CA. 4Rh-3 carries CA-Q110D mutation in addition to h4/5L and h6/7L from SIVmac239 CA. Viral infectivity was measured by luciferase activity in infected cells and presented as RLU. Naïve CRFK and CRFK cells expressing TRIM5α were infected with an equal amount of viruses generating 10^7 RLU in naïve cells. As shown in Fig. 4B, the infectivity of 5R and 4-8 for cells expressing CyM TRIM5α was similar to that of a negative control 5R/4-3. However, higher infectivity was observed for 5RS and 4-8S relative to 5R and 4-8. These results were consistent with previous reports that h4/5L and h6/7L in HIV-1 CA are a part of determinant for TRIM5α restriction [20,36]. The sensitivity of 4Rh-3 to TRIM5α was similar to that of 5RS and 4-8S. This indicates that CA-Q110D did not contribute to increase the resistance to TRIM5α. It has been reported that CyM TRIMCyp has the ability to restrict HIV-1 replication [15]. To examine the susceptibility of HIV-1mt variants to TRIMCyp, we generated feline CRFK cells expressing TRIMCyp, and the cells were infected with pseudotyped viruses as described above. As shown in Fig. 4C, all the clones tested were more resistant to a similar extent to TRIMCyp than the control 5R/4-3. In agreement with a previous study showing that elimination of alanine at position 88 within h4/5L of HIV-1 CA confers the resistance on the virus to TRIMCyp [15], our results indicate that the replacement of HIV-1 CA h4/5L with that of SIVmac239 is sufficient for HIV-1mt to evade from the TRIMCyp restriction. Second, we performed another susceptibility assay using the recombinant SeV expression system. This system assures a very high expression level of target proteins in cells infected with the recombinant SeV. Therefore, the ability of viruses to completely counteract the restriction effect of TRIM5 proteins could be determined by MT4/SeV-TRIM5 expression system. Human MT4 cells were infected with recombinant SeV expressing CyM TRIM5α, TRIMCyp, or SPRY(−)TRIM5, and then super-infected with HIV-1

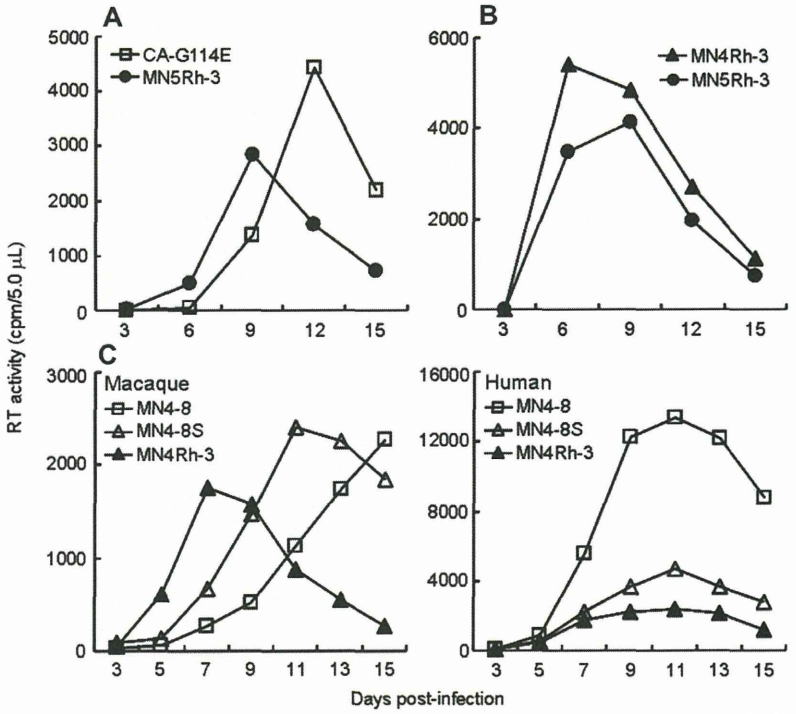

Fig. 3. Effect of CA modification on viral growth in macaque and human lymphocyte cell lines. (A and B) Growth kinetics of HIV-1mt clones carrying CA-G114E or CA-Q110D (MN5Rh-3 and MN4Rh-3) in CyM HSC-F cells. Virus samples were prepared from 293T cells transfected with the indicated proviral clones, and equal amounts (5×10^5 RT units) were inoculated into HSC-F cells (10^6). Virus replication was monitored by RT activity released into the culture supernatants. (C) Growth kinetics of MN4-8, MN4-8S, and MN4Rh-3 in HSC-F (Macaque) and MT4/CCR5 (Human) cells. Virus samples were prepared from 293T cells transfected with the indicated proviral clones, and equal amounts (10^6 RT units) were inoculated into HSC-F cells (10^6). For spinoculation of MT4/CCR5 cells (10^6), 6×10^5 RT units were used as inocula. Virus replication was monitored by RT activity released into the culture supernatants.

(NL4-3), SIVmac239, or HIV-1mt variants. SPRY(−)TRIM5 which can not bind to viral CA served as control. NL4-3 and SIVmac239 also served as controls for viral replication. As shown in Fig. 4D, NL4-3 replicated in cells expressing SPRY(−)TRIM5, but not in TRIM5α and TRIMCyp expressing cells. SIVmac239 exhibited similar growth kinetics in SPRY(−)TRIM5, TRIM5α and TRIMCyp expressing cells. All HIV-1mt variants replicated in TRIMCyp expressing cells similarly well in SPRY(−)TRIM5 cells. Together with assays in CRFK cells, these results showed that all HIV-1mt variants except for 5R/4-3 completely evade from TRIMCyp restriction. In contrast, the growth of all HIV-1mt variants was inhibited in CyM TRIM5α expressing MT4 cells. These results indicate that HIV-1mt variants do not evade from TRIM5α restriction as effectively as SIVmac239.

Results obtained by our two assay systems with respect to the susceptibility of HIV-1mt variants to CyM TRIM5α were apparently different (Fig. 4B and D), but this difference is most likely to be due to the TRIM5α expression level. In MT4 cells infected with recombinant SeV, TRIM5α is expressed at much higher level than that in transduced CRFK cells, masking the increase of resistance to TRIM5α detectable by the transduced CRFK system (Fig. 4B). Indeed, the growth enhancement of 5RS relative to 5R [20] can be explained by the results in Fig. 4B but not those in Fig. 4D. The apparent discrepancy of the sensitivity depending on TRIM5α expression level was also observed between B-LCL cells and transduced CRFK cells [41]. In sum, we can conclude here that MN4Rh-3 exhibits a partial resistance to TRIM5α insufficient for complete evasion as 5RS and 4-8S do, and that the CA-Q110D mutation is irrelevant to this property.

3.5. CA-Q110D enhances viral infectivity for macaque cells

Results so far showed that CA-Q110D does not contribute to evasion from TRIM5 proteins restriction in rather artificial systems using feline and human cells (Fig. 4). To investigate further how CA-Q110D enhances viral replication, we examined single-cycle viral infectivity in macaque cells. CyM kidney MK.P3(F) cells, which have heterozygote for TRIM5α and TRIMCyp, were infected with various VSV-G pseudoviruses and analyzed for their infectivity as described above. As shown in Fig. 5A, viral infectivity was increased by modification of h4/5L (compare 5R/4-3 and 5R&4-8). Modification of h6/7L in addition to h4/5L further augmented viral infectivity (compare 5R&4-8 and 5RS&4-8S). Introduction of the CA-Q110D mutation into 4-8S clone gave the highest infectivity among the viruses tested (see 4Rh-3). The results in

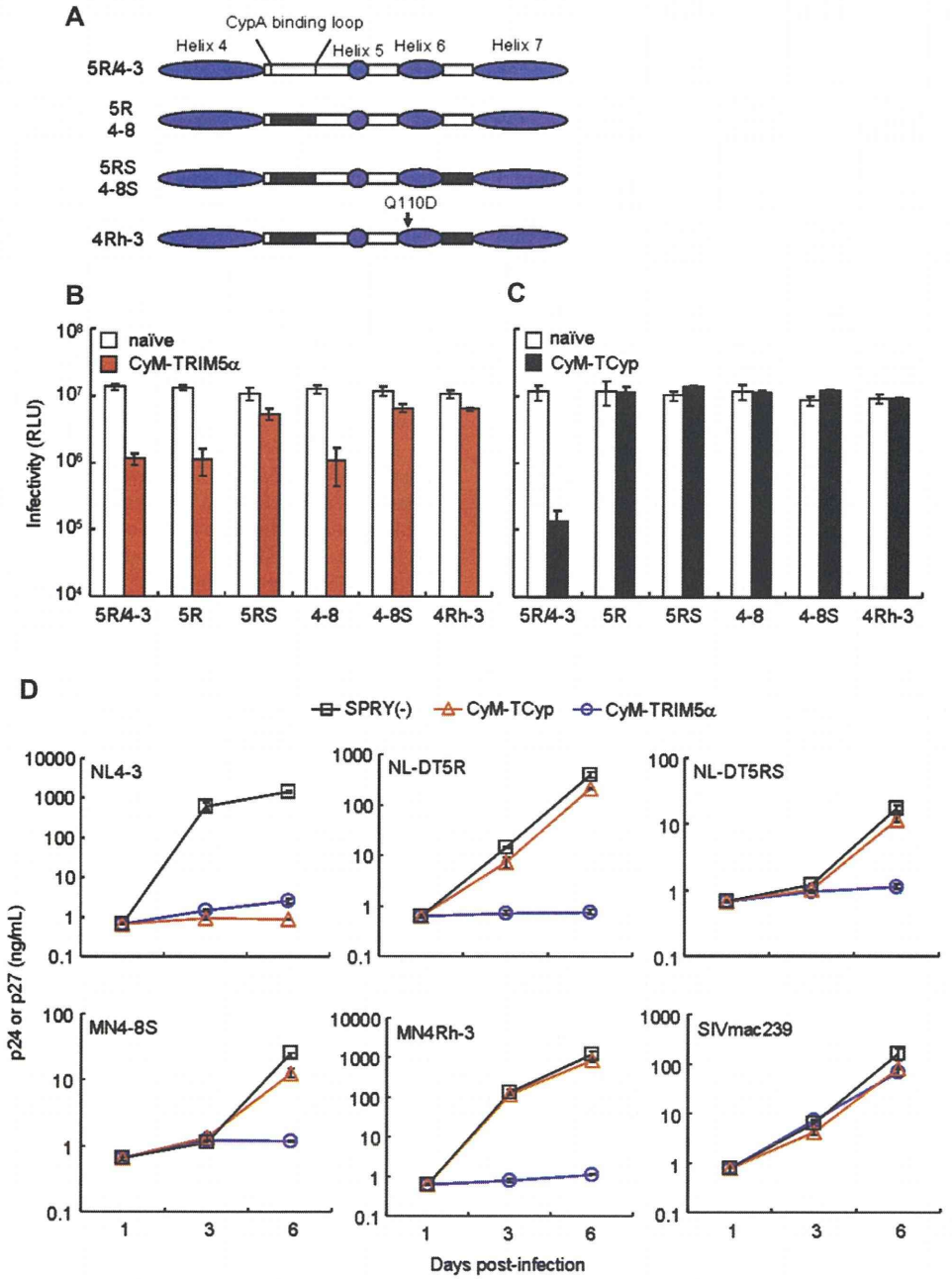

Fig. 4. Effect of CA modification in HIV-1mt variants on viral infectivity. (A) CA structure of viral clones used in TRIM5α/TRIMCyp susceptibility assays. Blue and white areas show helices and loops from HIV-1 NL4-3 CA, respectively. Sequences from SIVmac239 are indicated by black areas. (B and C) Susceptibility of HIV-1mt variants to CyM TRIM5 proteins as examined by CRFK system. Results for CyM TRIM5α (B) and for CyM TRIMCyp (TCyp) (C) are shown. VSV-G pseudotyped viruses were prepared from transfected 293T cells as input samples. Viruses generating 10^7 RLU in CRFK-naïve cells were inoculated into CRFK cells that express CyM TRIM5α or CyM TCyp. On day 2 post-infection, cells were analyzed for luciferase activity by a luminometer. (D) Susceptibility of HIV-1mt variants to CyM TRIM5 proteins as examined by SeV system. Human MT4 cells (10^5) were infected with recombinant SeV expressing CyM TRIM5α, TRIMCyp, or SPRY (−) TRIM5. Nine hours after infection, cells were super-infected with 20 ng (Gag-p24) of HIV-1 NL4-3, various HIV-1mt clones, or 20 ng (Gag-p27) of SIVmac239. Virus replication was monitored by the amount of Gag-p24 from NL4-3 and HIV-1mt clones or Gag-p27 from SIVmac239 in the culture supernatants. Error bars show actual fluctuations between duplicate samples. Data from one representative of three independent experiments are shown.

Fig. 5A show that CA-Q110D uniquely increases viral infectivity in macaque cells not observed in the other experimental systems (Fig. 4), and suggest that some factor(s) in CyM cells other than TRIM5α and TRIMCyp proteins is associated with this enhancement.

As shown in Fig. 5B, MN4Rh-3 displayed slower growth kinetics relative to those of SIVmac239 (note the peak day of virus production), although it grew better than the other HIV-1mt clones in CyM HSC-F cells. Approximately 100-fold more input virus (RT units) compared to SIVmac239 was required for MN4Rh-3 to exhibit similar growth kinetics with SIVmac239 (data not shown). These results have shown that even MN4Rh-3 grows more poorly in macaque cells than a standard SIVmac clone pathogenic for macaque monkeys.

4. Discussion

In this study, we have demonstrated that a single CA mutation (Q110D) greatly promotes HIV-1mt growth in macaque cells (Fig. 3). This enhancing effect was afforded independently of TRIM5 proteins restriction. The virus carrying the CA-Q110D mutation (MN4Rh-3) certainly overcame the anti-viral action of CyM TRIMCyp but not completely CyM TRIM5α. However, the mutation itself (Fig. 1) did not influence anti-TRIMCyp/TRIM5α activity of MN4Rh-3 reported here (Fig. 4). Notably, this mutation exquisitely enhanced viral growth in macaque cells (Fig. 3) by augmenting viral single-cycle infectivity (Fig. 5). The viral growth enhancement reported here is well reproduced in CyM peripheral blood mononuclear cells and in CyMs (manuscript in preparation).

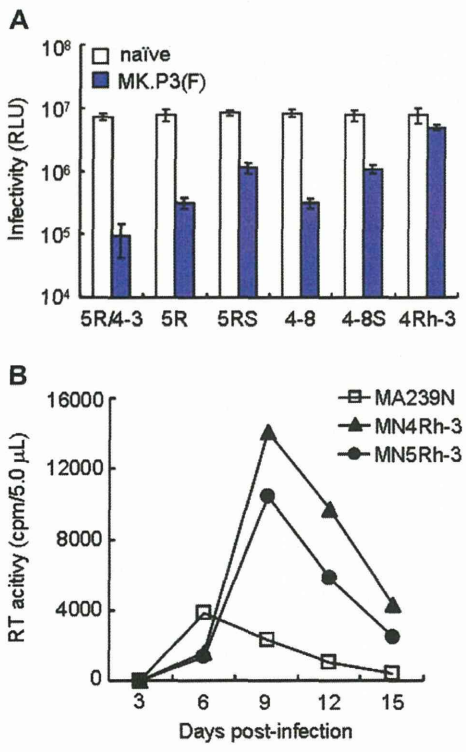

Fig. 5. Replication ability of various viruses in CyM cells. (A) Single-cycle infectivity of various HIV-1mt clones in CyM kidney MK.P3(F) cells. VSV-G pseudotyped viruses indicated were prepared from transfected 293T cells. MK.P3(F) cells were infected with an equal titer of viruses giving 10^7 RLU in CRFK-naïve cells. On day 2 post-infection, cells were analyzed for luciferase activity by a luminometer. (B) Multi-cycle growth kinetics of SIVmac and HIV-1mt viruses in CyM lymphocyte HSC-F cells. Virus samples were prepared from 293T cells transfected with the indicated proviral clones, and equal amounts (10^4 RT units) were inoculated into HSC-F cells (10^6). Virus replication was monitored by RT activity released into the culture supernatants. MA239N, an infectious clone of SIVmac239 with *nef*-open.

Regarding the mechanism for enhancement of viral growth by CA-Q110D, we initially thought a possibility that CA-Q110D compensates the disadvantage in HIV-1mt genome resulted from replacement of HIV-1 CA h4/5L and h6/7L with those of SIVmac239. However, this is highly unlikely because the enhancing effect is macaque cell-dependent (Fig. 3). Most feasible explanation is that CA-Q110D contributes to evade from a negative factor(s) in macaque cells such as CypA. Because HIV-1mt CA was designed not to bind to CypA, and the interaction between the two molecules was indeed undetectable by monitoring CypA virion-incorporation [18,20], we analyzed the binding by computer-assisted structural modeling. Homology modeling of the CA-CypA complexes was performed based on the crystal structure of HIV-1 CA NTD bound to CypA (PDB code: 1M9C [28]), and the binding energies, E_{bind}, were calculated using MOE as described previously [42,43]. As shown in Fig. 6, HIV-1 (NL4-3) CA was predicted to interact with CypA via its h4/5L (binding energy: −64.4 kcal/mol). The binding energy of CA and CypA was decreased by CA modifications, such as h4/5L replacement (NL-DT5R: −31.0 kcal/mol), h4/5L and h6/7L replacement (NL-DT5RS: −36.1 kcal/mol), and Q110D substitution in addition to h4/5L and h6/7L replacement (MN4Rh-3: −30.1 kcal/mol). Decrease in E_{bind} in NL-DT5R is consistent with the result that the h4/5L region directly interacts with CypA [28]. Notably, the E_{bind} for the NL-DT5RS CA was greater than that of the NL-DT5R and MN4Rh-3 CAs. These results suggest that not only h6/7L replacement but also Q110D substitution can influence structure of CypA binding surface of CA. The Q110D substitution is located on the exposed surface of helix 6 connecting to the h6/7L (Fig. 2B). CA helix 6 has been reported to interact with CypA binding region on h4/5L through hydrogen bonding [44,45]. Thereby it is reasonable that the local electrostatic change on the helix 6 by the Q110D substitution influenced structures of h4/5L via changes in fluctuation and conformation of h6/7L. This in turn could lead to reduction in stability of the MN4Rh-3 CA-CypA complex compared with NL-DT5RS CA-CypA complex, as predicted in Fig. 6. Our computer-assisted structural study suggests that the Q110D substitution can induce electrostatic modulation of the overall CA surface structure including h4/5L and h6/7L. Similar modulation mechanism of binding surface structures via charged amino acid substitution at distant site from the binding surface has been reported for Cyp domain of CyM TRIMCyp [15] and CD4 binding site of HIV-1 gp120 outer

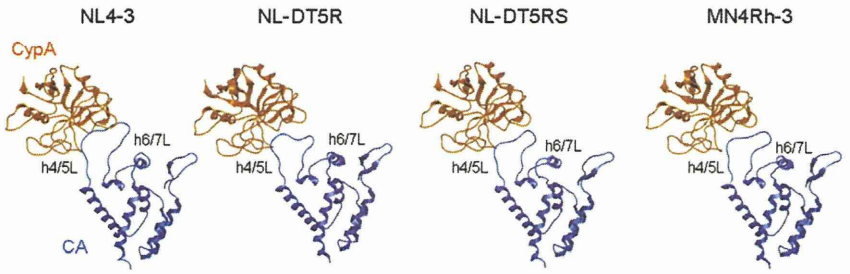

	NL4-3	NL-DT5R	NL-DT5RS	MN4Rh-3
CA	HIV-1 CA	h4/5L from SIVmac239	h4/5L and h6/7L from SIVmac239	h4/5L and h6/7L from SIVmac239 and Q110D
Binding energy (kcal/mol)	-64.447	-31.012	-36.071	-30.051

Fig. 6. Structural models of HIV CA NTD bound to CypA. The model of CA NTD bound to CypA was constructed by homology modeling using the crystal structure of HIV-1 CA NTD and CypA complex (PDB code: 1M9C [28]). The binding energies, E_{bind} (kcal/mol), of the complex were calculated using MOE as described previously [42,43]. The formula $E_{bind} = E_{complex} - (E_{CA} + E_{CypA})$ was used for the E_{bind} calculation, where $E_{complex}$ is the energy of the CA/CypA complex models, E_{CA} is the energy of the CA monomer model, and E_{CypA} is the energy of the CypA monomer model.

domain [46]. Thus, it is not unreasonable to assume that the replication of MN4Rh-3 carrying CA-Q110D is enhanced in macaque cells but reduced in human cells by augmenting its dissociation from CypA (Fig. 6). However, it was found to be difficult to experimentally confirm this structural insight by determining the effect of cyclosporine A or of siRNA against CypA on viral infectivity because interaction between the HIV-1mt CA and CypA was so weak. Alternatively, CA-Q110D may contribute to the alteration of the affinity to unknown anti-CA factor(s) other than CypA and TRIM5 proteins. In this case, it is speculated that the factor(s) might act negatively on HIV-1 replication in macaque cells but positively in human cells, and vice versa. Further study is required to elucidate the mechanism for enhancement of viral growth potential by CA-Q110D.

In conclusion, further modification of the HIV-1mt genome is necessary to overcome unconquered replication block(s) present in macaque cells and obtain viral clones similarly replication-competent in macaque cells and pathogenic for animals with SIVmac (Fig. 5). Considering the genome structure of MN4Rh-3 and the results presented here, major targets for modification now are *gag*-CA (against TRIM5α) and *vpu* (against tetherin). Gag-CA is one of the two principal viral determinants (CA and Vif) for the HIV-1 species-tropism. Construction of HIV-1 CA that evades from TRIM5α restriction is also useful for elucidation of the less-defined CA-TRIM5α interaction and antiviral mechanism of TRIM5α. Tetherin, identified as anti-virion release factor, is antagonized by Vpu [47,48], but macaque tetherin was not counteracted by HIV-1 Vpu [49]. Construction of HIV-1 Vpu that down-modulate macaque tetherin may enhance viral replication *in vivo* as well as *in vitro* [50]. Through these approaches, we may be able to precisely analyze HIV-1 replication and pathogenesis *in vivo* and provide new strategies against HIV-1/AIDS.

Acknowledgments

This study was supported by a grant from the Ministry of Health, Labor and Welfare of Japan (Research on HIV/AIDS project no. H23-003).

References

[1] M.H. Malim, M. Emerman, HIV-1 accessory proteins—ensuring viral survival in a hostile environment, Cell Host Microbe 3 (2008) 388–398.
[2] F. Kirchhoff, Immune evasion and counteraction of restriction factors by HIV-1 and other primate lentiviruses, Cell Host Microbe 8 (2010) 55–67.
[3] R. Shibata, H. Sakai, M. Kawamura, K. Tokunaga, A. Adachi, Early replication block of human immunodeficiency virus type 1 in monkey cells, J. Gen. Virol. 76 (1995) 2723–2730.
[4] M. Nomaguchi, N. Doi, K. Kamada, A. Adachi, Species barrier of HIV-1 and its jumping by virus engineering, Rev. Med. Virol. 18 (2008) 261–275.
[5] M. Nomaguchi, A. Adachi, Virology as biosystematics: towards understanding the viral infection biology, Front. Microbiol. 1 (2010) 2.
[6] R.K. Holmes, M.H. Malim, K.N. Bishop, APOBEC-mediated viral restriction: not simply editing? Trends Biochem. Sci. 32 (2007) 118–128.
[7] H. Huthoff, G.J. Towers, Restriction of retroviral replication by APOBEC3G/F and TRIM5alpha, Trends Microbiol. 16 (2008) 612–619.
[8] K. Strebel, J. Luban, K.T. Jeang, Human cellular restriction factors that target HIV-1 replication, BMC Med. 7 (2009) 48.
[9] J. Luban, Cyclophilin A, TRIM5, and resistance to human immunodeficiency virus type 1 infection, J. Virol. 81 (2007) 1054–1061.
[10] G.J. Towers, The control of viral infection by tripartite motif proteins and cyclophilin A, Retrovirology 4 (2007) 40.
[11] E.E. Nakayama, T. Shioda, Anti-retroviral activity of TRIM5 alpha, Rev. Med. Virol. 20 (2010) 77–92.
[12] R.M. Newman, L. Hall, M. Connole, G.L. Chen, S. Sato, E. Yuste, W. Diehl, E. Hunter, A. Kaur, G.M. Miller, W.E. Johnson, Balancing selection and the evolution of functional polymorphism in old world monkey TRIM5alpha, Proc. Natl. Acad. Sci. U. S. A. 103 (2006) 19134–19139.
[13] S.J. Wilson, B.L. Webb, L.M. Ylinen, E. Verschoor, J.L. Heeney, G.J. Towers, Independent evolution of an antiviral TRIMCyp in rhesus macaques, Proc. Natl. Acad. Sci. U. S. A. 105 (2008) 3557–3562.

[14] A.J. Price, F. Marzetta, M. Lammers, L.M. Ylinen, T. Schaller, S.J. Wilson, G.J. Towers, L.C. James, Active site remodeling switches HIV specificity of antiretroviral TRIMCyp, Nat. Struct. Mol. Biol. 16 (2009) 1036–1042.
[15] L.M. Ylinen, A.J. Price, J. Rasaiyaah, S. Hué, N.J. Rose, F. Marzetta, L.C. James, G.J. Towers, Conformational adaptation of Asian macaque TRIMCyp directs lineage specific antiviral activity, PLoS Pathog. 6 (2010) e1001062.
[16] K. Kamada, T. Igarashi, M.A. Martin, B. Khamsri, K. Hatcho, T. Yamashita, M. Fujita, T. Uchiyama, A. Adachi, Generation of HIV-1 derivatives that productively infect macaque monkey lymphoid cells, Proc. Natl. Acad. Sci. U. S. A. 103 (2006) 16959–16964.
[17] T. Igarashi, R. Iyengar, R.A. Byrum, A. Buckler-White, R.L. Dewar, C.E. Buckler, H.C. Lane, K. Kamada, A. Adachi, M.A. Martin, Human immunodeficiency virus type 1 derivative with 7% simian immunodeficiency virus genetic content is able to establish infections in pig-tailed macaques, J. Virol. 81 (2007) 11549–11552.
[18] K. Kamada, T. Yamashita, K. Hatcho, A. Adachi, M. Nomaguchi, Evasion from CypA- and APOBEC-mediated restrictions is insufficient for HIV-1 to efficiently grow in simian cells, Microbes Infect. 11 (2009) 164–171.
[19] A. Saito, M. Nomaguchi, S. Iijima, A. Kuroishi, T. Yoshida, Y.J. Lee, T. Hayakawa, K. Kono, E.E. Nakayama, T. Shioda, Y. Yasutomi, A. Adachi, T. Matano, H. Akari, Improved capacity of a monkey-tropic HIV-1 derivative to replicate in cynomolgus monkeys with minimal modifications, Microbes Infect. 13 (2011) 58–64.
[20] A. Kuroishi, A. Saito, Y. Shingai, T. Shioda, M. Nomaguchi, A. Adachi, H. Akari, E.E. Nakayama, Modification of a loop sequence between alpha-helices 6 and 7 of virus capsid (CA) protein in a human immunodeficiency virus type 1 (HIV-1) derivative that has simian immunodeficiency virus (SIVmac239) vif and CA alpha-helices 4 and 5 loop improves replication in cynomolgus monkey cells, Retrovirology 6 (2009) 70.
[21] T. Yamashita, N. Doi, A. Adachi, M. Nomaguchi, Growth ability in simian cells of monkey cell-tropic HIV-1 is greatly affected by downstream region of the vif gene, J. Med. Invest. 55 (2008) 236–240.
[22] M. Yamashita, M. Emerman, Capsid is a dominant determinant of retrovirus infectivity in nondividing cells, J. Virol. 78 (2004) 5670–5678.
[23] J.S. Lebkowski, S. Clancy, M.P. Calos, Simian virus 40 replication in adenovirus-transformed human cells antagonizes gene expression, Nature 317 (1985) 169–171.
[24] H. Akari, T. Fukumori, S. Iida, A. Adachi, Induction of apoptosis in herpesvirus saimiri-immortalized T lymphocytes by blocking interaction of CD28 with CD80/CD86, Biochem. Biophys. Res. Commun. 263 (1999) 352–356.
[25] N. Doi, S. Fujiwara, A. Adachi, M. Nomaguchi, Growth ability in various macaque cell lines of HIV-1 with simian cell-tropism, J. Med. Invest. 57 (2010) 284–292.
[26] A. Adachi, H.E. Gendelman, S. Koenig, T. Folks, R. Willey, A. Rabson, M.A. Martin, Production of acquired immunodeficiency syndrome-associated retrovirus in human and nonhuman cells transfected with an infectious molecular clone, J. Virol. 59 (1986) 284–291.
[27] U. O'Doherty, W.J. Swiggard, M.H. Malim, Human immunodeficiency virus type 1 spinoculation enhances infection through virus binding, J. Virol. 74 (2004) 10074–10080.
[28] B.R. Howard, F.F. Vajdos, S. Li, W.I. Sundquist, C.P. Hill, Structural insights into the catalytic mechanism of cyclophilin A, Nat. Struct. Biol. 10 (2003) 475–481.
[29] N. Deshpande, K.J. Addess, W.F. Bluhm, J.C. Merino-Ott, W. Townsend-Merino, Q. Zhang, C. Knezevich, L. Xie, L. Chen, Z. Feng, R.K. Green, J.L. Flippen-Anderson, J. Westbrook, H.M. Berman, P.E. Bourne, The RCSB protein data bank: a redesigned query system and relational database based on the mmCIF schema, Nucleic Acids Res. 33 (Database issue) (2005) D233–D237.
[30] H. Song, E.E. Nakayama, M. Yokoyama, H. Sato, J.A. Levy, T. Shioda, A single amino acid of the human immunodeficiency virus type 2 capsid affects its replication in the presence of cynomolgus monkey and human TRIM5alphas, J. Virol. 81 (2007) 7280–7285.
[31] K. Kono, H. Song, M. Yokoyama, H. Sato, T. Shioda, E.E. Nakayama, Multiple sites in the N-terminal half of simian immunodeficiency virus capsid protein contribute to evasion from rhesus monkey TRIM5α-mediated restriction, Retrovirology 7 (2010) 72.
[32] N. Inagaki, H. Takeuchi, M. Yokoyama, H. Sato, A. Ryo, H. Yamamoto, M. Kawada, T. Matano, A structural constraint for functional interaction between N-terminal and C-terminal domains in simian immunodeficiency virus capsid proteins, Retrovirology 7 (2010) 90.
[33] P. Labute, The generalized Born/volume integral implicit solvent model: estimation of the free energy of hydration using London dispersion instead of atomic surface area, J. Comput. Chem. 29 (2008) 1693–1698.
[34] J.W. Ponder, D.A. Case, Force fields for protein simulations, Adv. Protein Chem. 66 (2003) 27–85.
[35] A. Onufriev, D. Bashford, D.A. Case, Modification of the generalized Born model suitable for macromolecules, J. Phys. Chem. B 104 (2000) 3712–3720.
[36] T.Y. Lin, M. Emerman, Determinants of cyclophilin A-dependent TRIM5 alpha restriction against HIV-1, Virology 379 (2008) 335–341.
[37] A. Kuroishi, K. Bozek, T. Shioda, E.E. Nakayama, A single amino acid substitution of the human immunodeficiency virus type 1 capsid protein affects viral sensitivity to TRIM5 alpha, Retrovirology 7 (2010) 58.
[38] M. Stremlau, C.M. Owens, M.J. Perron, M. Kiessling, P. Autissier, J. Sodroski, The cytoplasmic body component TRIM5alpha restricts HIV-1 infection in old world monkeys, Nature 427 (2004) 848–853.
[39] Z. Keckesova, L.M. Ylinen, G.J. Towers, Cyclophilin A renders human immunodeficiency virus type 1 sensitive to old world monkey but not human TRIM5 alpha antiviral activity, J. Virol. 80 (2006) 4683–4690.
[40] E. Sokolskaja, L. Berthoux, J. Luban, Cyclophilin A and TRIM5alpha independently regulate human immunodeficiency virus type 1 infectivity in human cells, J. Virol. 80 (2006) 2855–2862.
[41] S.Y. Lim, T. Rogers, T. Chan, J.B. Whitney, J. Kim, J. Sodroski, N.L. Letvin, TRIM5alpha modulates immunodeficiency virus control in rhesus monkeys, PLoS Pathog. 6 (2010) e1000738.
[42] C.O. Onyango, A. Leligdowicz, M. Yokoyama, H. Sato, H. Song, E.E. Nakayama, T. Shioda, T. de Silva, J. Townend, A. Jaye, H. Whittle, S. Rowland-Jones, M. Cotten, HIV-2 capsids distinguish high and low virus load patients in a West African community cohort, Vaccine 28 (2010) B60–B67.
[43] M. Kinomoto, R. Appiah-Opong, J.A. Brandful, M. Yokoyama, N. Nii-Trebi, E. Ugly-Kwame, H. Sato, D. Ofori-Adjei, T. Kurata, F. Barre-Sinoussi, T. Sata, K. Tokunaga, HIV-1 proteases from drug-naive West African patients are differentially less susceptible to protease inhibitors, Clin. Infect. Dis. 41 (2005) 243–251.
[44] R.K. Gitti, B.M. Lee, J. Walker, M.F. Summers, S. Yoo, W.I. Sundquist, Structure of the amino-terminal core domain of the HIV-1 capsid protein, Science 273 (1996) 231–235.
[45] C. Tang, Y. Ndassa, M.F. Summers, Structure of the N-terminal 283-residue fragment of the immature HIV-1 Gag polyprotein, Nat. Struct. Biol. 9 (2002) 537–543.
[46] M. Yokoyama, S. Naganawa, K. Yoshimura, S. Matsushita, H. Sato, Structural dynamics of HIV-1 envelope Gp120 outer domain with V3 loop, PLoS One 7 (2012) e37530.
[47] S.J. Neil, T. Zang, P.D. Bieniasz, Tetherin inhibits retrovirus release and is antagonized by HIV-1 Vpu, Nature 451 (2008) 425–430.
[48] N. Van Damme, D. Goff, C. Katsura, R.L. Jorgenson, R. Mitchell, M.C. Johnson, E.B. Stephens, J. Guatelli, The interferon-induced protein BST-2 restricts HIV-1 release and is downregulated from the cell surface by the viral Vpu protein, Cell Host Microbe 3 (2008) 245–252.
[49] D. Sauter, M. Schindler, A. Specht, W.N. Landford, J. Münch, K.A. Kim, J. Votteler, U. Schubert, F. Bibollet-Ruche, B.F. Keele, J. Takehisa, Y. Ogando, C. Ochsenbauer, J.C. Kappes, A. Ayouba, M. Peeters, G.H. Learn, G. Shaw, P.M. Sharp, P. Bieniasz, B.H. Hahn, T. Hatziioannou, F. Kirchhoff, Tetherin-driven adaptation of Vpu and Nef function and the evolution of pandemic and nonpandemic HIV-1 strains, Cell Host Microbe 6 (2009) 409–421.
[50] M. Shingai, T. Yoshida, M.A. Martin, K. Strebel, Some human immunodeficiency virus type 1 Vpu proteins are able to antagonize macaque BST-2 in vitro and in vivo: Vpu-negative simian-human immunodeficiency viruses are attenuated in vivo, J. Virol. 85 (2011) 9708–9715.

nature
structural &
molecular biology

The APOBEC3C crystal structure and the interface for HIV-1 Vif binding

Shingo Kitamura[1,2], Hirotaka Ode[1], Masaaki Nakashima[1,2], Mayumi Imahashi[1,3], Yuriko Naganawa[1], Teppei Kurosawa[1,2], Yoshiyuki Yokomaku[1], Takashi Yamane[2], Nobuhisa Watanabe[2,4], Atsuo Suzuki[2], Wataru Sugiura[1,3] & Yasumasa Iwatani[1,3]

The human apolipoprotein B mRNA-editing enzyme catalytic polypeptide–like 3 (APOBEC3, referred to as A3) proteins are cellular cytidine deaminases that potently restrict retrovirus replication. However, HIV-1 viral infectivity factor (Vif) counteracts the antiviral activity of most A3 proteins by targeting them for proteasomal degradation. To date, the structure of an A3 protein containing a Vif-binding interface has not been solved. Here, we report a high-resolution crystal structure of APOBEC3C and identify the HIV-1 Vif–interaction interface. Extensive structure-guided mutagenesis revealed the role of a shallow cavity composed of hydrophobic or negatively charged residues between the α2 and α3 helices. This region is distant from the DPD motif (residues 128–130) of APOBEC3G that participates in HIV-1 Vif interaction. These findings provide insight into Vif-A3 interactions and could lead to the development of new pharmacologic anti–HIV-1 compounds.

The A3 family of cytidine deaminases consists of cellular proteins that prevent the mobilization of diverse retroviruses, retrotransposons and other viral pathogens (reviewed in ref. 1). In humans, seven members of this protein family, A3A, A3B, A3C, A3DE, A3F, A3G and A3H, are encoded in a tandem array on chromosome 22 (ref. 2). The A3 proteins are characterized by the presence of one or two conserved zinc-coordinating domains (Z domains) consisting of $HXE(X)_{23-28}CXXC$ motifs (reviewed in ref. 3). On the basis of phylogenetic analyses, the Z domains fall into three types: Z1 (A3A and the C-terminal domains (CTDs) of A3B and A3G), Z2 (A3C, both halves of A3DE and A3F, and the N-terminal domains (NTDs) of A3B and A3G) and Z3 (A3H)[2]. The Z2 domain can be further subdivided into three subgroups on the basis of amino acid sequences: the A3F NTD (the NTDs of A3B, A3DE and A3F), the A3G NTD and the A3F CTD (A3C and the CTDs of A3DE and A3F) subgroups.

HIV-1 Vif protein overcomes the antiviral activity of A3 proteins in infected cells by forming an E3 ubiquitin ligase complex, with cullin 5, elongin B (EloB) and elongin C (EloC) in collaboration with core-binding factor β (CBF-β)[4,5], which subsequently leads to A3 degradation through the ubiquitin-proteasome pathway[6–8]. Thus, the elimination of A3 in cells during virus production prevents its encapsidation into progeny HIV-1 viruses. A3 degradation specificity is determined by the ability of Vif to bind to the target. HIV-1 Vif binds A3C, A3DE, A3F, A3G and A3H but not A3A and A3B. Among the Z domains, only Z3 (A3H haplotype II) and Z2 (the A3G NTD and the A3F CTD subgroups) contain a critical interface that interacts with HIV-1 Vif[9–11].

One specific residue of the human A3G NTD responsible for the Vif interaction, Asp128, was primarily identified by comparative studies of species-specific A3G-Vif interactions[12–15]. Subsequently, extensive mutational analyses of amino acids adjacent to Asp128 revealed that the 128-Asp-Pro-Asp-130 (DPD) motif of A3G, located at loop 7 between β4 and α4, is crucial for the direct interaction with Vif[16]. These critical residues in the A3G NTD have been mapped to a variable-loop structure in close proximity to the nucleic acid–binding surface. In contrast, two independent studies have reported that two residues that are critical for the Vif interaction, Glu289 and Glu324 of the A3F CTD, are situated in the α3 and α4 helices, respectively, which are located distally from the DPD motif[10,17]. Despite our knowledge of these critical A3 residues, the structural features underlying the Vif-interaction interface on A3 proteins have not been previously elucidated.

To date, the three-dimensional structure of only the A3G CTD has been determined by NMR[18,19] or X-ray crystallography[20,21]. The structures of full-length A3 or the domain involved in the HIV-1 Vif–binding interface have not been previously solved. Here, we present the first report, to our knowledge, of the crystal structure of full-length human A3C. We used extensive structure-guided mutagenesis to explore the residues that form the HIV-1 Vif–binding interface. Our results demonstrate that ten residues of A3C are critical for the formation of the Vif-interaction interface, which mapped to a different region from loop 7 that corresponds to an area of the DPD motif in the A3G NTD. Furthermore, our data indicate that the responsible interface provides a shallow cavity composed of hydrophobic or

[1]Clinical Research Center, Department of Infectious Diseases and Immunology, National Hospital Organization Nagoya Medical Center, Nagoya, Japan. [2]Department of Biotechnology, Graduate School of Engineering, Nagoya University, Nagoya, Japan. [3]Program in Integrated Molecular Medicine, Graduate School of Medicine, Nagoya University, Nagoya, Japan. [4]Synchrotron Radiation Research Center, Nagoya University, Nagoya, Japan. Correspondence should be addressed to Y.I. (iwataniy@nnh.hosp.go.jp).

Received 23 April; accepted 7 August; published online 23 September 2012; doi:10.1038/nsmb.2378

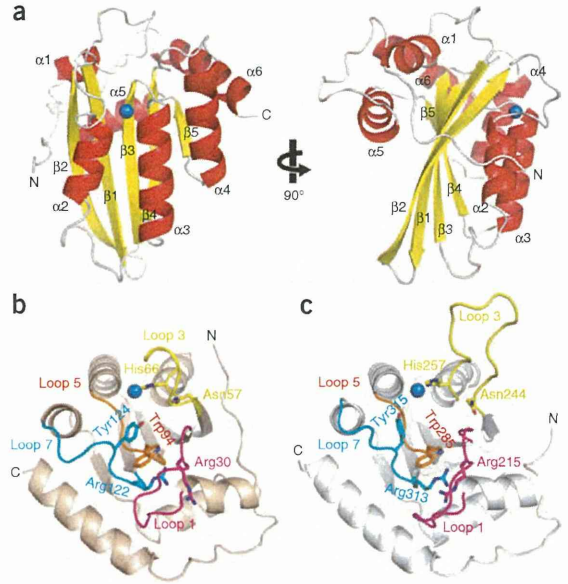

Figure 1 The X-ray crystal structure of full-length A3C. (**a**) Two views of the A3C structure, rotated by 90°, are shown. The α-helices (α1–α6) and β-strands (β1–β5) are colored in red and yellow, respectively. A coordinated zinc ion is represented as a blue sphere. (**b**,**c**) Structural comparison around the catalytic groove of A3C (**b**) and A3G CTD (**c**). Amino acid side chains of the conserved residues in loop 1 (magenta), loop 3 (yellow), loop 5 (orange) and loop 7 (cyan) are labeled with the residue numbers.

negatively charged residues. In addition, we found that the structural features of the Vif-binding interfaces are conserved in the homologous Z2-type A3C, A3F and A3DE proteins but not in the A3G protein. These results will deepen our understanding of A3-Vif interactions and aid in the development of new strategies using potential endogenous inhibitors against HIV-1.

RESULTS

High-resolution crystal structure of full-length A3C

Initially, human A3C was expressed in *Escherichia coli* as an N-terminal GST-tagged recombinant protein to increase its solubility. The tag was subsequently removed. We further purified the full-length A3C protein (residues 1–190) and solved its structure at 2.15 Å (**Fig. 1a** and **Table 1**). The A3C structure has a core platform composed of six α-helices (α1–α6) and five β-strands (β1–β5), with a coordinated zinc ion that is well conserved in the cytidine deaminase superfamily[22]. The superimposition of the A3C core onto that of the A3G CTD crystal structure (PDB 3IR2) for 86% of the backbone atoms exhibited a Cα r.m.s. deviation of 1.36 Å, thereby indicating the structural conservation of the core platform.

In contrast to the high conservation of the core structures, the loop regions, particularly loops 1, 3, 4 and 7 of the A3C and A3G CTD structures, are distinct (**Fig. 1b**,**c** and **Supplementary Fig. 1a**,**b**). Nevertheless, the positions of certain residues in the loops exhibit structural similarity. Arg30, Asn57, His66, Trp94, Arg122 and Tyr124 in A3C (**Fig. 1b**) are similar to Arg215, Asn244, His257, Trp285, Arg313 and Tyr315 in the A3G CTD (**Fig. 1c**). These residues primarily have critical roles in maintaining the conformation of the catalytic center and the groove involved in substrate binding[18,20], which are functionally conserved features among A3 proteins. In contrast, differences in the HIV-1 Vif interaction are attributable to unique conformational differences between the A3C and A3G CTD structures.

Notably, the A3C structure exhibits a continuous well-ordered β2-strand that is remarkably different from that of the A3G CTD (PDB 3IR2) (**Fig. 1** and **Supplementary Fig. 1a**,**b**). Molecular dynamics (MD) simulations support the high stability of the A3C β2 (**Supplementary Fig. 1c–f**), which is also observed in the APOBEC2 (A2) crystal structure[23]. In the A2 structure, a continuous β2 strand mediates dimerization through a β2 of another molecule. However, we did not detect any intermolecular contacts through the β2-β2 interaction within the 20 largest contacts in the crystal packing (**Supplementary Fig. 2a**). In addition, our dynamic light-scattering experiments indicated both monomodal and bimodal distributions of A3C proteins in solution (**Supplementary Fig. 2b**), although our gel-filtration data indicated that most of the protein was distributed in the monomer size fraction (**Supplementary Fig. 2c**). These results suggest that dynamic A3C dimerization might occur but not through their β2 strands. This effect might be partly owing to 13 amino acids of the N-terminal region, which reside on the β2 strand, that sterically hinder the β2-β2 associations. Recently, a similar observation with a full-length A2 structure has also been reported[24].

Ten A3C residues are critical for HIV-1 Vif binding

To determine the interface for HIV-1 Vif recognition of A3C, extensive structure-guided mutagenesis experiments were performed by using an approach analogous to that previously described for A3G[25]. A single

Table 1 Data collection and refinement statistics

	APOBEC3C
Data collection	
Space group	$P6_1$
Cell dimensions	
a, *b*, *c* (Å)	105.04, 105.04, 70.05
α, β, γ (°)	90, 90, 120
Resolution (Å)	105–2.15 (2.19–2.15)
R_{merge}	5.4 (33.8)
$I / \sigma I$	94.5 (13.3)
Completeness (%)	99.9 (100)
Redundancy	22.3 (22.6)
Refinement	
Resolution (Å)	91–2.15
No. reflections	22,783
R_{work} / R_{free}	21.4 / 26.3
No. atoms	3,281
Protein	3,188
Ligand/ion	3
Water	90
B factors	45.56
Protein	45.69
Ligand/ion	45.50
Water	40.90
R.m.s. deviations	
Bond lengths (Å)	0.012
Bond angles (°)	1.390

A single crystal was used for solving the structure. Values in parentheses are for highest-resolution shell.